FACULTY OF MECHANICAL ENGINEERING CTU IN PRAGUE

DEPARTMENT OF ENVIRONMENTAL ENGINEERING

UNIVERSITY CENTRE FOR ENERGY EFFICIENT BUILDINGS CTU IN PRAGUE

TITLE

TRNSYS TYPE 207

MODEL OF DUAL PURPOSE SOLAR COLLECTOR BASED ON DETAILED CONSTRUCTION PARAMETERS AND ENERGY BALANCE

AUTHORS

Viacheslav Shemelin

Tomáš Matuška

Bořivoj Šourek

PAGES 31

ANNEXES 1

DATE December 2017

Contents

1. Introduction

Among the solar thermal technology, the flat-plate solar collectors have been widely used as liquid solar collectors or air solar collectors. The idea to combine both types of technology for development of dual function solar collector in not new. It has emerged from the typical situation for mild and cold climatic zone, where solar radiation is sufficient for preparation of hot water for households needs (50-60 °C) in summer, whereas the output temperatures from solar collectors in winter generally do not reach values higher than 30 °C, however, it can be sufficient, for example, for pre-heating of fresh air. Such integrated design allows to increase an annual energy yield of solar system and to maximize the operating time, which makes it more cost-effective than the conventional water or air systems.

The presented Type 207 is a detailed mathematical model developed for thermal performance simulations of two different solar collector designs. The considered designs of dual function solar collector are shown in Fig. 1: Design 1 - It is a absorber pipe upper bond configuration with single air flow between absorber and bottom plate; Design 2 - It is a absorber pipe upper bond configuration with single air flow between absorber and transparent insulation.

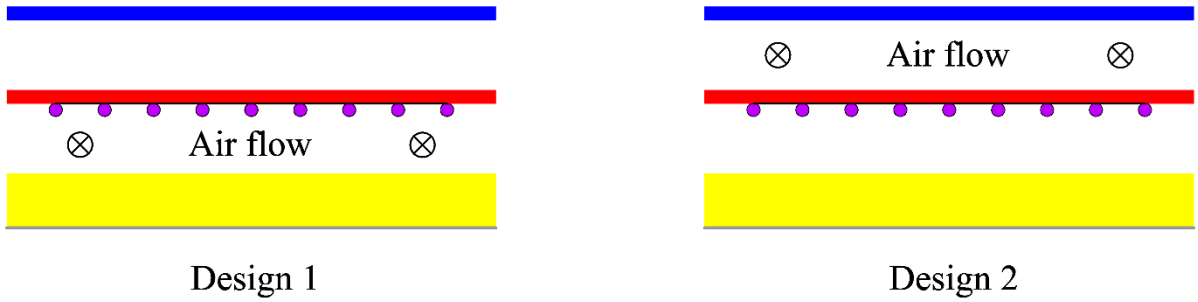

Fig. 1 – The considered solar air collector desings

The dual solar collector can be specified by a number of detailed parameters, optical properties of the transparent cover and the absorber and thermophysical properties of main components of the solar collector. Moreover, the transparent cover (glazing, plastic or another transparent insulation structure) and the back thermal insulation are defined by temperature dependent thermal conductance.

The implementation of the model in TRNSYS environment offers the parametric analysis for different construction alternatives for annual solar collector performance in the given solar system application. There is also a possibility to change mathematical models describing the fundamental heat transfer phenomena (natural convection, wind convection, forced convection, etc.) and perform sensitivity analysis for selection of the models.

Note that the presented model does not imply simultaneous work of liquid and air part. It means that dual funcition solar collecor model operates either as a liquid collector or as an air collector, depends on the input – Operating Mode. If Operating Mode is equal to 0, the model operates as a liquid collector and if is equal to 1 it operates as an air collector. In fact Type 207 has emerged on the basis of combining the two already existing models in TRNSYS – Type 205 (flat-plate solar liquid collector) [1] and Type 206 (flat-plate solar air collector) [2].

2. Parameter-List

Nr.	*short*	*explanation*	*unit*	*range*
1	A	Collector width	*m*	[0;inf]
2	B	Collector height	*m*	[0;inf]
3	C	Collector length	*m*	[0;inf]
4	A_{abs}	Absorber area	m^2	[0;inf]
5	a_f	Front air channel width	*m*	[0;inf]
6	b_f	Front air channel height	*m*	[0;inf]
7	c_f	Front air channel length	*m*	[0;inf]
8	a_b	Back air channel width	*m*	[0;inf]
9	b_b	Back air channel height	*m*	[0;inf]
10	c_b	Back air channel length	*m*	[0;inf]
11	ε_{c2}	External surface emissivity of cover (f_2)	[-]	[0;1]
12	ε_{c1}	Internal surface emissivity of cover (f_1)	[-]	[0;1]
13	$\varepsilon_{abs,f}$	Front surface emissivity of absorber	[-]	[0;1]
14	$\varepsilon_{abs,b}$	Back surface emissivity of absorber	[-]	[0;1]
15	ε_{ins}	Internal surface emissivity of insulation (b_1)	[-]	[0;1]
16	ε_{fs}	External surface emissivity of frame (b_2)	[-]	[0;1]
17	ε_{as}	Emissivity of adjacent surfaces	[-]	[0;1]
18	τ_n	Solar transmittance of the collector cover	[-]	[0;1]
19	α_{abs}	Solar absorptance of the absorber	[-]	[0;1]
20	d_{abs}	Thickness of the absorber	*mm*	[0;inf]
21	λ_{abs}	Thermal conductivity of the absorber	*W/m.K*	[0;inf]
22	W	Distance between riser pipes	*mm*	[0;inf]
23	L	Length of riser pipes	*m*	[0;inf]
24	D_e	Riser pipe external diameter	*mm*	[0;inf]
25	D_i	Riser pipe internal diameter	*mm*	[0;inf]
26	a	Average bond width	*mm*	[0;inf]
27	b	Average bond thickness	*mm*	[0;inf]
28	λ_b	Bond thermal conductivity	*W/m.K*	[0;inf]
29	P	Number of riser pipes	[-]	[0;inf]
30	b_0	1st-order incidence angle modifier (IAM)	[-]	[0;1]
31	b_1	2nd-order incidence angle modifier (IAM)	[-]	[-1;1]
32	h_{cov0}	Thermal conductance of cover 0	$W/m^2.K$	[0;inf]
33	h_{cov1}	Thermal conductance of cover 1	$W/m^2.K^2$	[-inf;inf]
34	h_{cov2}	Thermal conductance of cover 2	$W/m^2.K^3$	[-inf;inf]
35	h_{ins0}	Thermal conductance of back insulation 0	$W/m^2.K$	[0;inf]
36	h_{ins1}	Thermal conductance of back insulation 1	$W/m^2.K^2$	[-inf;inf]
37	h_{ins2}	Thermal conductance of back insulation 2	$W/m^2.K^3$	[-inf;inf]
38	M_1	Dual function collector Design	[-]	[1;2]
39	M_2	Wind convection model Mode	[-]	[1;4]
40	M_3	Natural convection model Mode	[-]	[1;6]
41	M_4	Heat transfer fluids model Mode	[-]	[1;3]
42	M_5	Glycol mass concentration	[%]	[0;100]
43	M_6	Laminar convection in pipes model Mode	[-]	[1;5]
44	M_7	Turbulent convection heat transfer in pipes model Mode	[-]	[1;6]

Parameter list *(Continued)*

45	M_8	Calculation Mode	[-]	[1;2]
46	M_9	Forced convection model Mode	[-]	[1;7]

3. Input-List

Nr.	***short***	***explanation***	***unit***	***range***
1	O	Operating Mode	[-]	[0;1]
2	t_{in}	Inlet liquid temperature	$°C$	[inf;+inf]
3	$\dot{M}$	Inlet liquid flowrate	kg/h	[0;inf]
4	t_{in}	Inlet air temperature	$°C$	[-inf;+inf]
5	$\dot{M}$	Inlet air flowrate	kg/h	[0;inf]
6	t_{amb}	Ambient temperature	$°C$	[-inf;+inf]
7	t_{sky}	Sky temperature	$°C$	[-inf;+inf]
8	I_{beam}	Beam radiation for collector surface	$kJ/h.m^2$	[0;inf]
9	I_{sky}	Sky diffuse radiation for collector surface	$kJ/h.m^2$	[0;inf]
10	I_{gnd}	Ground reflected diffuse radiation for collector surface	$kJ/h.m^2$	[0;inf]
11	θ	Incidence angle	deg	[0;+inf]
12	φ	Collector slope	deg	[0;90]
13	w	Wind velocity	m/s	[0;+inf]

4. Output-List

Nr.	***short***	***explanation***	***unit***	***range***
1	t_{in}	Outlet liquid temperature	$°C$	[inf;+inf]
2	$\dot{M}$	Outlet liquid flowrate	kg/h	[0;inf]
3	t_{out}	Outlet air temperature	$°C$	[-inf;+inf]
4	$\dot{M}$	Outlet air flowrate	kg/h	[0;inf]
5	Φ_{out}	Useful energy gain of collector	kJ/h	[-inf;+inf]
6	η	Collector thermal efficiency	[-]	[0;1]
7	t_{abs}	Absorber mean temperature	$°C$	[-inf;+inf]

5. Units conversion

In the table above, there are several non-SI units. The presented Type 207 computes in the SI units, which are more convenient for calculations. Therefore all non-SI units have to be converted into SI units. The conversion of some non-SI units into SI units is given in Tab. 1.

Tab. 1 – Conversation of non-SI units

Dimension	**Non-SI unit**	**Equivalence in SI-units**
Temperature	t [°C]	$\vartheta = t + 273.15$ [K]
Mass flow	$\dot{M}$ [kg/h]	$\dot{m} = \frac{\dot{M}}{3600}$ [kg/s]
Energy flux	I [kJ/h.m^2]	$G = \frac{I}{3.6}$ [W/m^2]
Power	Φ_{out} [kJ/h]	$\dot{Q}_u = \frac{\Phi_{out}}{3.6}$ [W]

6. Operation mode = 0 (Solar liquid collector)

The core of the Operation mode = 0 is a mathematical model for solar flat-plate liquid collector solving one-dimensional heat transfer balances. Hottel and Woertz [3], Hottel and Whilier [4] and Bliss [5] developed the simplest assumptions: thermal capacitances are neglected and a single value of collector overall heat loss coefficient is considered, which depends on collector characteristics (geometry, mass flow rate, efficiency itself etc.), average plate temperature and external conditions (air, temperature and external heat transfer coefficient). Based on these assumptions and considering that the heat transfer is mainly one-dimensional and predominant in the direction normal to the flow plane, Duffie and Beckman [6] developed a simplified model to characterize the solar collector in steady state conditions.

The mathematical model in general consists of two parts: external energy balance of absorber (heat transfer from absorber surface to ambient environment) and internal energy balance of absorber (heat transfer from absorber surface into heat transfer fluid). Model solves the energy balance of the solar collector under steady-state conditions according to principle Hottel-Whillier equation for usable thermal power

$$\dot{Q}_u = A_{abs} F_R \left[\tau_n \alpha_{abs} G_t - U\left(\vartheta_{in} - \vartheta_{amb}\right)\right] \quad \text{[W]} \qquad (1)$$

The main planes of the collector are cover exterior surface (f_2), cover interior surface (f_1), absorber (*abs*), back insulation interior surface (b_1), back frame exterior surface (b_2), edge insulation interior surface (e_1) and edge frame exterior surface (e_2). Ambient environment is labeled with (*amb*). A surface temperature is determined for each plane of collector during the calculation procedure. The main collector planes are schematically outlined in Fig. 2.

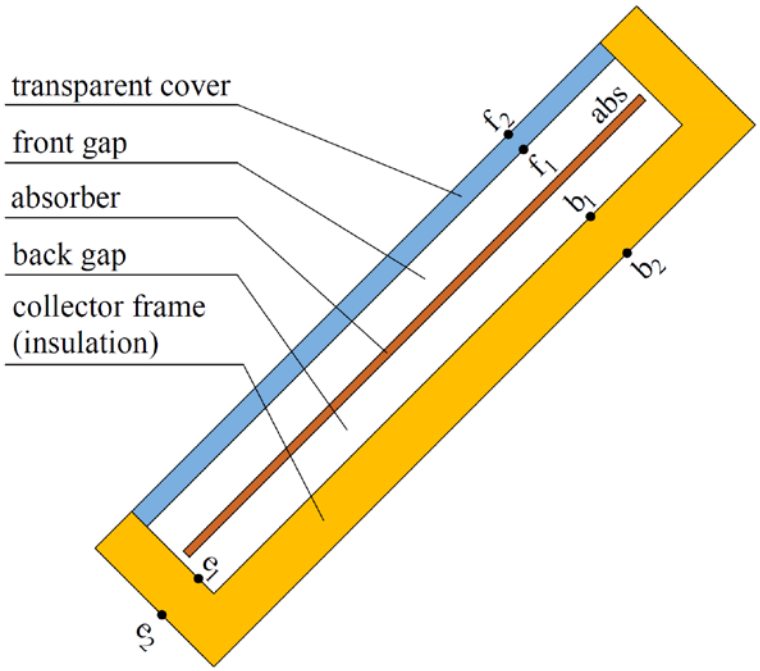

Fig. 2 – Main temperature planes (surfaces) in solar collector model

6.1. External energy balance

The external energy balance consists of:

1) the heat transfer by radiation and by natural convection in the gap between absorber surface and transparent cover (respectively back insulation and edge insulation);
2) the heat transfer by conduction through transparent cover (respectively back insulation and edge insulation);
3) the heat transfer convection and radiation from exterior cover (respectively back frame and edge frame) surface to ambient.

To calculate the heat transfer coefficients properly, temperatures for main collector planes (surfaces) should be known, but on the other side the temperature distribution in the collector is dependent on the heat transfer coefficients values. Therefore, external energy balance of absorber is solved in an iteration loop starting from first estimate of temperatures for each main surface based on given input temperature ϑ_{in} and ambient temperature ϑ_{amb}. The absorber temperature ϑ_{abs} required in the calculation is estimated in first iteration loop of external balance from ϑ_{in} by relationship:

$$\vartheta_{abs} = \vartheta_{in} + 10 \qquad [\mathrm{K}] \tag{2}$$

Then for the calculation of heat transfer coefficients between main collector surfaces (f_1, f_2, b_1, b_2, e_1, e_2), the surface temperatures are needed, but at the start of calculation process the temperatures are not known. In the first iteration step, surface temperatures are estimated from temperature difference between absorber and ambient environment uniformly as follows:

$$\vartheta_{f1} = \vartheta_{b1} = \vartheta_{e1} = \vartheta_{abs} - \frac{\vartheta_{abs} - \vartheta_{amb}}{3} \qquad [\mathrm{K}] \tag{3}$$

$$\vartheta_{f2} = \vartheta_{b2} = \vartheta_{e2} = \vartheta_{amb} + \frac{\vartheta_{abs} - \vartheta_{amb}}{3} \qquad [\mathrm{K}] \tag{4}$$

After that heat transfer coefficients can be calculated and collector heat loss coefficients U_f, U_b and U_e can be obtained.

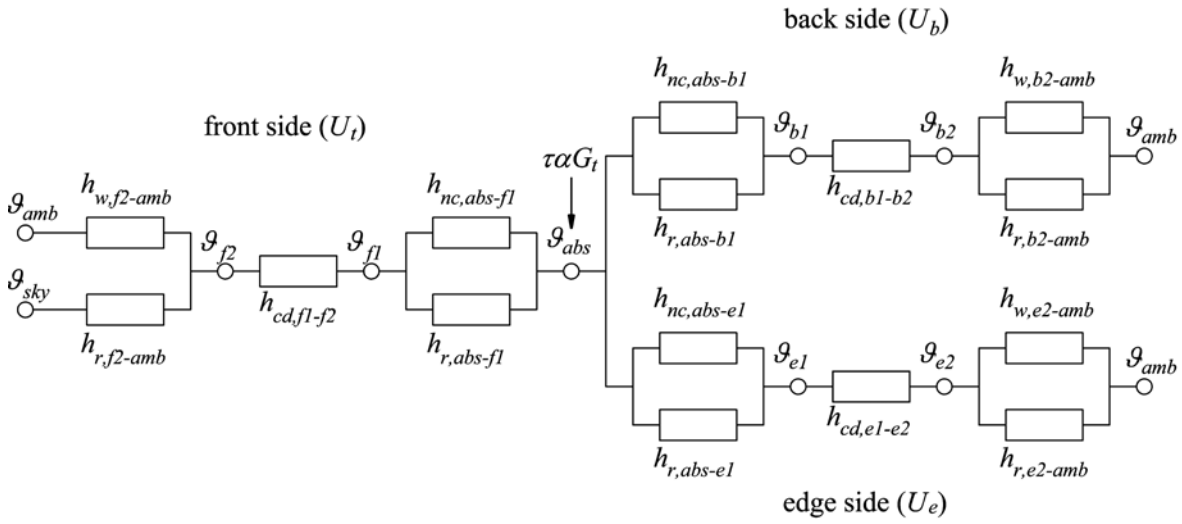

Fig. 3 – Schematic detailed layout of external energy balance of absorber

6.1.1. Radiation heat transfer between top surface and sky

To describe the radiation heat transfer between top surface and sky, the sky area is considered as a black body of equivalent temperature ϑ_{sky}. Equivalent sky temperature ϑ_{sky} is introduced due to fact that sky temperature is not uniform and constant and atmosphere radiates only in certain wavelengths ranges in reality.

Radiation heat transfer coefficient is given by

$$h_{r,f2-amb} = \varepsilon_{f2}\sigma\frac{\vartheta_{f2}^4 - \vartheta_{sky}^4}{\vartheta_{f2} - \vartheta_{amb}} \quad [\mathrm{W/m^2.K}] \tag{5}$$

where

σ is Stefan-Boltzmann constant, $\sigma = 5.67\times10^{-8}$ W/m^2.K^4.

6.1.2. Wind convection heat transfer from top, bottom and edge surfaces to ambient

Heat transfer by convection from exterior surface of transparent cover, back side or edge side to ambient environment under realistic conditions (mixed natural and forced wind convection) is quite problematic. A large number of relationships and correlations derived from experiments, more or less reproducing the boundary conditions of solar collector installation, can be found in literature (see Tab. 2).

Tab. 2 – Wind convection correlations

M2	**Author**	**Equation**	**Range**
1	McAdams [7]	$h_{w,s-amb} = 5.7 + 3.8w$ $h_{w,s-amb} = 6.47w^{0.78}$	for w < 5 m/s for w > 5 m/s
2	Watmuff [8]	$h_{w,s-amb} = 2.3 + 3.0w$	0 < w < 7 m/s
3	Test [9,10]	$h_{w,s-amb} = 8.55 + 2.56w$	0 < w < 5 m/s
4	Kumar [11]	$h_{w,s-amb} = 10.03 + 4.687w$	0 < w < 4 m/s

6.1.3. Conduction through transparent cover and insulation material

For a single cover glazing the conductance can be considered as a constant and calculated as

$$h_{cd,f1-f2} = \frac{\lambda}{d_{f1-f2}} \quad [\mathrm{W/m^2.K}] \tag{6}$$

where

λ thermal conductivity of cover, W/m.K;

$d_{fl\text{-}f2}$ thickness of cover, m.

In the case of transparent insulation material or in the case of back insulation, thermal conductance of the structure could be determined as a function of mean temperature $\vartheta_{s1\text{-}s2}$

$$h_{cd,s1-s2} = f(\vartheta_{s1-s2}) = h_{cov0} + h_{cov1}\vartheta_{s1-s2} + h_{cov2}\vartheta_{s1-s2}^2 \quad [\mathrm{W/m^2.K}] \tag{7}$$

6.1.4. Natural convection in closed gas layer between absorber and transparent cover

Heat transfer by natural convection in the closed gas layer between absorber and transparent cover is characterized by Nusselt number Nu related to characteristic dimension of the layer, the thickness b_f. Geometric parameters of the gas layer and heat flow direction (upward) are outlined in Fig. 4.

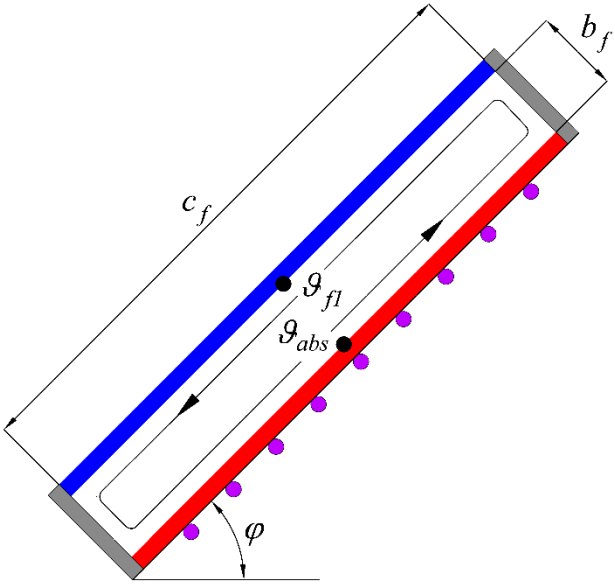

Fig. 4 – Natural convection in closed gas layer

Natural convection heat transfer coefficient for closed inclined layer between absorber and cover glazing can be obtained from

$$h_{nc} = \frac{\mathrm{Nu}\lambda_g}{b_f} \quad [\mathrm{W/m^2.K}] \tag{8}$$

where

λ_g is thermal conductivity of still gas for mean temperature $\vartheta_{abs\text{-}f1}$ in the gas layer, W/m.K.

Nusselt number for natural convection is dependent on Rayleigh number Ra, i.e. product of Grashof number Gr and Prandtl number Pr.

$$\mathrm{Ra} = \mathrm{Gr}\,\mathrm{Pr} \quad [-] \tag{9}$$

Prandtl number can be obtained from the properties of used gas at mean temperature of the layer $\vartheta_{abs\text{-}f1}$ as given

$$\mathrm{Pr} = \frac{\nu\rho c}{\lambda} \quad [-] \tag{10}$$

where

ν is kinematic viscosity of gas, $\mathrm{m^2/s}$;

ρ density of gas, $\mathrm{kg/m^3}$;

c specific thermal capacity of gas, J/kg.K.

Grashof number Gr_b is given by

$$\mathrm{Gr} = \frac{\beta g b_{f1}^3 \Delta\vartheta}{\nu^2} = \frac{1}{\vartheta_{abs-f1}} \frac{g b_{f1}^3 \left(\vartheta_{abs} - \vartheta_{f1}\right)}{\nu^2} \quad [-] \tag{11}$$

where

β is volumetric thermal expansion coefficient, 1/K;

g gravity acceleration, m/s^2.

Number of published experiments and derived correlations has been found for natural convection heat transfer in sloped enclosure (Tab. 3).

Tab. 3 – Selected correlations for natural convection in the sloped closed gas layer

M_3	Author	Equation	Range		
			Ra	φ	c_f/b_f
1	Hollands [12]	$\mathrm{Nu} = 1 + 1.44\left[1 - \frac{1708}{\mathrm{Ra}\cos\varphi}\right]^+ \left(1 - \frac{(\sin\varphi)^{1.6}\,1708}{\mathrm{Ra}\cos\varphi}\right) + \left[\left(\frac{\mathrm{Ra}\cos\varphi}{5830}\right)^{1/3} - 1\right]^+$	$0 < \mathrm{Ra} < 10^5$	0°-60°	cca 48
2	Buchberg [13]	$\mathrm{Nu}_b = 1 + 1.44\left[1 - \frac{1708}{\mathrm{Ra}\cos\varphi}\right]^+$ $\mathrm{Nu} = 0.229\left(\mathrm{Ra}\cos\varphi\right)^{0.252}$ $\mathrm{Nu} = 0.157\left(\mathrm{Ra}\cos\varphi\right)^{0.285}$	$1708 < \mathrm{Ra}\cos\varphi < 10^5$ $5900 < \mathrm{Ra}\cos\varphi < 9.2\times10^4$ $9.2\times10^4 < \mathrm{Ra}\cos\varphi < 10^6$	0°-60°	
3	Randal [14]	$\mathrm{Nu} = 0.118\left[\mathrm{Ra}\cos^2(\varphi - 45)\right]^{0.29}$	$2.8\times10^3 < \mathrm{Ra}\cos\varphi < 2.2\times10^5$	45°-90°	9-36
4	Schinkel [15]	$\mathrm{Nu} = a(\varphi)\mathrm{Ra}^{1/3}$	$10^5 < \mathrm{Ra}\cos\varphi < 4\times10^6$	0°-90°	6-27
5	Niemann [16]	$\mathrm{Nu} = 1 + \frac{m(\mathrm{Ra})^c}{\mathrm{Ra} + n}$	$10^2 < \mathrm{Ra} < 10^8$		
6	Matuska [17]	$\mathrm{Nu} = \left(0.1464 - 2.602\times10^{-4}\varphi - 2.046\times10^{-6}\varphi^2\right)\mathrm{Ra}^{0.29}$	integral correlation (see [5])		

φ	$a(\varphi)$
0°	0.080
10°	0.079
20°	0.075
30°	0.074
40°	0.074

φ	$a(\varphi)$
50°	0.074
60°	0.072
70°	0.069
80°	0.068
90°	0.062

φ	m	n	c
0°	0.0700	0.32×10^4	1.333
45°	0.0430	0.41×10^4	1.360
90°	0.0236	1.01×10^4	1.393

superscript + indicates that content of brackets is considered only for positive values, for negative values the content is equal to 0.

6.1.5. Radiation heat transfer between parallel plates

Radiation heat transfer coefficient between absorber and interior surface of transparent cover between absorber and insulation can be obtained from

$$h_{r,abs-s} = \frac{\sigma}{\frac{1}{\varepsilon_{abs}} + \frac{1}{\varepsilon_s} - 1} \frac{\vartheta_{abs}^4 - \vartheta_s^4}{\vartheta_{abs} - \vartheta_s} \quad [\mathrm{W/m^2.K}] \tag{12}$$

6.1.6. Natural convection between absorber and back insulation

Natural convection heat transfer coefficient in enclosed gas layer between absorber and insulation is given by similar equation as in 6.1.4. Geometric parameters of gas layer and heat flow direction (downward) are outlined in Fig. 5.

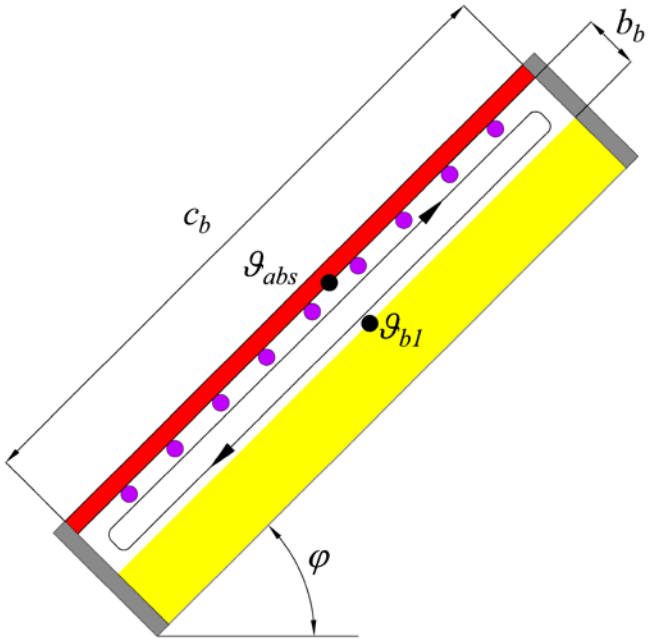

Fig. 5 – Natural convection in closed gas layer (heat flow downward)

$$h_{nc,abs-b1} = \frac{\mathrm{Nu}\lambda_g}{b_b} \qquad [\mathrm{W/m^2.K}] \tag{13}$$

where

λ_g is thermal conductivity of still gas for mean temperature $\vartheta_{abs\text{-}b1}$ in the gas layer, W/m.K.

A literature review has been done to find proper equation for heat transfer coefficient for the case of natural convection in gas enclosure (closed gas layer) with heat flow downward required. Only one general equation has been obtained. Arnold et al. [18] suggest correlation based on Nusselt number obtained for vertical gas layer (90°) as a sinus function in the range of 90-180° as given

$$\mathrm{Nu} = 1 + \left[\mathrm{Nu}\left(\varphi = 90^\circ\right) - 1\right] sin\left(180^\circ - \varphi\right) \qquad [-] \tag{14}$$

6.1.7. Radiation heat exchange between back and edge frame and adjacent ambient surfaces

Radiation heat transfer coefficient between exterior surface of collector back and edge frame and adjacent surfaces in ambient environment (roof) related to ambient temperature ϑ_{amb} can be expressed as

$$h_{r,s-amb} = \frac{\sigma}{\frac{1}{\varepsilon_{fs}} + \frac{1}{\varepsilon_{as}} - 1} \frac{\vartheta_s^4 - \vartheta_{amb}^4}{\vartheta_s - \vartheta_{amb}} \ [\mathrm{W/m^2.K}] \tag{15}$$

6.1.8. Radiation and convection heat exchange between absorber and edge insulation

The estimation of edge losses is complicated for most collectors. However the edge losses are small for a standard size of collector box and it is not necessary to predict them with great accuracy. According to Duffie and Beckman [6] the magnitudes of the thermal resistance of convection and radiation heat transfer between absorber and edge insulation are much smaller than that of conduction through edge insulation and heat transfer from the edge frame of the collector to surroundings. Therefore it can be assumed that the temperature of edge insulation ϑ_{e1} is equal to absorber temperature ϑ_{abs}.

6.1.9. Collector heat loss coefficient (*U-value*)

As illustrated in Fig. 3 heat loss coefficient for front side of the collector U_f can be determined as

$$U_f = \frac{1}{\frac{1}{h_{r,f2-amb} + h_{conv,f2-amb}} + \frac{1}{h_{cond,f1-f2}} + \frac{1}{h_{r,abs-f1} + h_{conv,abs-f1}}} \quad [\mathrm{W/m^2.K}] \tag{16}$$

By analogy, heat loss coefficient for back side U_b and for edge side U_e of the collector can be determined as

$$U_b = \frac{1}{\frac{1}{h_{r,b2-amb} + h_{conv,b2-amb}} + \frac{1}{h_{cond,b1-b2}} + \frac{1}{h_{r,abs-b1} + h_{conv,abs-b1}}} \quad [\mathrm{W/m^2.K}] \tag{17}$$

$$U_e = \frac{1}{\frac{1}{h_{r,e2-amb} + h_{conv,e2-amb}} + \frac{1}{h_{cond,e1-e2}}} \quad [\mathrm{W/m^2.K}] \tag{18}$$

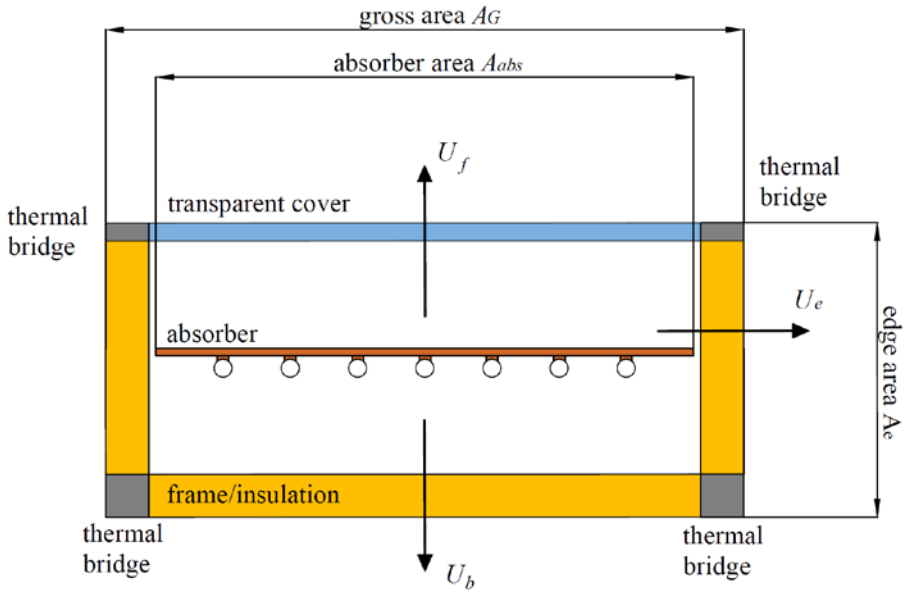

Fig. 6 – Collector heat loss with respect to aperture and gross area

Overall heat loss of solar collector (*U*-value) is related to gross dimensions (gross collector area A_G) as illustrated in Fig. 6 to cover the effect of thermal bridges not to underestimate the heat loss. On the other side, the usable heat output of the collector refers to absorber area A_{abs}, therefore overall collector heat loss coefficient *U* used in the internal energy balance calculations should be also related to absorber area A_{abs}.

The overall heat loss coefficient *U* based on absorber area can be obtain as

$$U = \left(U_f + U_b + U_e \frac{A_e}{A_G} \right) \frac{A_G}{A_{abs}} \qquad [\mathrm{W/m^2.K}] \tag{19}$$

6.1.10. Recalculation of surface temperatures

Since heat transfer and heat loss coefficients have been calculated for incorrect temperatures (first estimates), next iteration step should follow. From heat transfer coefficients and heat flows through front, back and edge side of the solar collector the temperature distribution can be obtained by reverse calculation process as follows

$$\vartheta_{f1} = \vartheta_{abs} - \frac{U_f \left(\vartheta_{abs} - \vartheta_{amb} \right)}{h_{r,abs-f1} + h_{nc,abs-f1}} \qquad [\mathrm{K}] \tag{20}$$

$$\vartheta_{f2} = \vartheta_{amb} + \frac{U_f \left(\vartheta_{abs} - \vartheta_{amb} \right)}{h_{r,f2-amb} + h_{w,f2-amb}} \qquad [\mathrm{K}] \tag{21}$$

Analogous to front side surface temperatures calculation, for back side and edge side can be applied

$$\vartheta_{b1} = \vartheta_{abs} - \frac{U_b \left(\vartheta_{abs} - \vartheta_{amb} \right)}{h_{r,abs-b1} + h_{n,abs-b1}} \qquad [\mathrm{K}] \tag{22}$$

$$\vartheta_{b2} = \vartheta_{amb} + \frac{U_b \left(\vartheta_{abs} - \vartheta_{amb} \right)}{h_{r,b2-amb} + h_{w,b2-amb}} \qquad [\mathrm{K}] \tag{23}$$

$$\vartheta_{e1} = \vartheta_{abs} \qquad [\mathrm{K}] \tag{24}$$

$$\vartheta_{e2} = \vartheta_{amb} + \frac{U_e \left(\vartheta_{abs} - \vartheta_{amb} \right)}{h_{r,e2-amb} + h_{w,e2-amb}} \qquad [\mathrm{K}] \tag{25}$$

The new and more correct values of surface temperatures are used in next iteration step for calculation of individual heat transfer coefficients between the surfaces and new and more correct value of heat loss coefficient *U* (see Fig. 3).

6.2. Internal energy balance

The internal energy balance considers:

1) fin heat transfer by conduction;
2) heat transfer by conduction through the bond between absorber and pipes;
3) heat transfer by forced convection from interior surface of pipe to fluid.

Internal energy balance proceeds in its own iteration loop with respect to relative dependence between mean fluid temperature ϑ_{mean} and forced convection heat transfer coefficients in absorber pipe register.

In the first iteration cycle of internal energy balance, the mean fluid temperature is estimated from ϑ_{in} by relationship:

$$\vartheta_{mean} = \vartheta_{in} + 10 \qquad [\mathrm{K}] \qquad (26)$$

With use of this first estimate of mean fluid temperature ϑ_{mean} the collector efficiency factor F', collector heat removal factor F_R, usable thermal power and efficiency of solar collector can be calculated.

6.2.1. Fin efficiency F

When considered absorber element as a fin, it is convenient to introduce the concept of fin efficiency given by

$$F = \frac{\tanh\left[m(W-2a)/2\right]}{m(W-2a)/2} \qquad [-] \qquad (27)$$

where

$$m = \sqrt{\frac{U}{\lambda_{abs} d_{abs}}} \qquad [-] \qquad (28)$$

6.2.2. Collector efficiency factor F'

Except the conduction heat transfer by the fin, also conduction through the bond fin-pipe and heat transfer from pipe to liquid by forced convection influence the overall heat transfer from absorber surface to heat transfer liquid. Collector or absorber efficiency factor F' is introduced to describe how "efficient" the heat transfer from absorber surface to heat transfer fluid is. For the most used upper bond configuration of absorber (Fig. 7) the efficiency factor is given as

$$F' = \frac{1/U}{W\left[\frac{1}{U\left[2a+(W-2a)F\right]} + \frac{1}{C_b} + \frac{1}{h_i \pi D_i}\right]} \qquad [-] \qquad (29)$$

where

h_i is forced convection heat transfer coefficient in riser pipe, W/m^{2}K.

C_b bond thermal conductance calculated from

$$C_b = \frac{\lambda_b a}{b} \qquad [\mathrm{W/m.K}] \qquad (30)$$

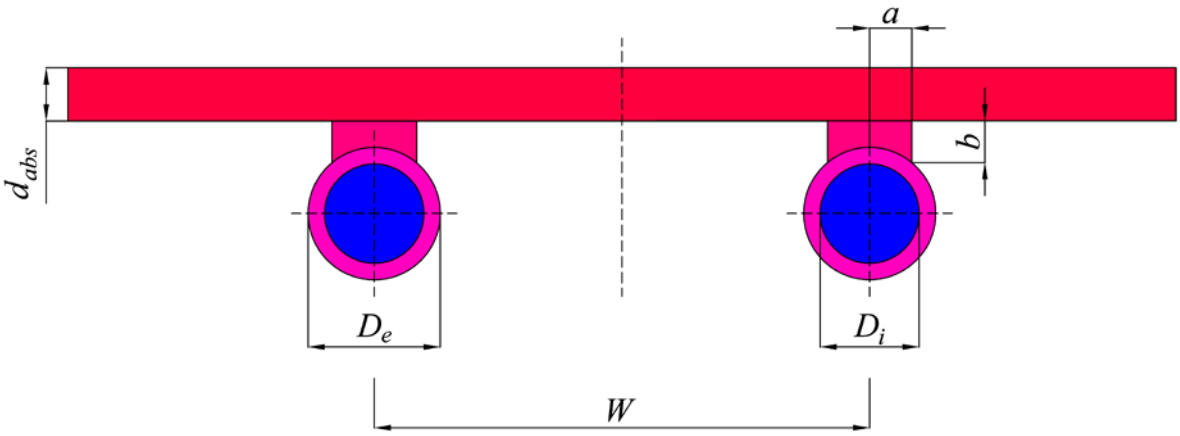

Fig. 7 – Absorber-pipe upper bond configuration

6.2.3. Forced convection heat transfer in pipes (h_i)

Forced convection heat transfer coefficient between the fluid and wall in absorber riser pipe is determined from Nusselt number

$$h_i = \mathrm{Nu}_D \frac{\lambda_f}{D_i} \qquad [\mathrm{W/m^2K}] \tag{31}$$

where

λ_f is thermal conductivity of heat transfer fluid, W/m.K.

Laminar forced convection heat transfer in circular pipes is widely described in literature. Tab. 4 shows correlations for Nusselt number for laminar forced convection heat transfer found in literature. In the case of developing flow, dimensionless longitudinal coordinate x^* is defined as inverse value of Graetz number characterizing the laminar flow in pipes as given in equation

$$x^* = \mathrm{Gz}^{-1} = \frac{L/D_i}{\mathrm{Re}_D \,\mathrm{Pr}} \quad [-] \tag{32}$$

Tab. 4 – Correlations for laminar forced convection heat transfer in pipes

M6	**Author**	**Equation**	**Conditions**
1	Shah [18]	$\mathrm{Nu}_D = 4.364$	fully developed velocity and temperature profile, constant heat flux
2	Shah [18]	$\mathrm{Nu}_D = 1.953 x^{*-1/3}$ $\quad x^* \le 0.03$ $\mathrm{Nu}_D = 4.364 + \frac{0.0722}{x^*}$ $\quad x^* > 0.03$	entry region of length L, developing profile, constant heat flux
3	Hausen [19]	$\mathrm{Nu}_D = 3.66 + \frac{0.668(D/L)\mathrm{Re}_D \,\mathrm{Pr}}{1 + 0.04[(D/L)\mathrm{Re}_D \,\mathrm{Pr}]^{2/3}}$	entry region of length L, developing profile

Tab. 4 (Continued)

4	Sieder-Tate [20]	$\mathrm{Nu}_D = 1.86\left(\frac{1}{x^*}\right)^{1/3}\left(\frac{\mu}{\mu_w}\right)$	entry region - thermally and hydraulically developing flow 0.48 < Pr < 16700 $0.0044 < \left(\frac{\mu}{\mu_w}\right) < 9.75$ recommended for $\left(\frac{1}{x^*}\right)^{1/3}\left(\frac{\mu}{\mu_w}\right)^{0.14} > 2$ else fully developer profile
5	Churchill and Ozoe [21]	$\mathrm{Nu}_D = \frac{2 \cdot 0.6366\left[(4/\pi)x*\right]^{-1/2}}{\left[1+\left(\mathrm{Pr}/0.0468\right)^{2/3}\right]^{1/4}}$	entry region - thermally and hydraulically developing flow Pr > 2 $10^{-7} < x < 10^{-3}$

In the case of turbulent flow, different set of equations (see Tab. 5) is applicable to calculation of the Nusselt number, mostly in the form

$$\mathrm{Nu}_D = A\mathrm{Re}_D^m \mathrm{Pr}^n \text{ [-]} \qquad (33)$$

The turbulent flow inside the riser pipes of solar collectors is very rare when using antifreeze water-glycol mixtures as heat transfer fluid with high viscosity.

Tab. 5 – Correlations for laminar forced convection heat transfer in pipes

M7	**Author**	**Equation**	**Conditions**
1	Colburn [22]	$\mathrm{Nu}_D = 0.023\,\mathrm{Re}_D^{4/5}\,\mathrm{Pr}^{1/3}$	$2x10^4 < \mathrm{Re}_D < 10^6$
2	Dittus-Boelter [23]	$\mathrm{Nu}_D = 0.023\,\mathrm{Re}_D^{4/5}\,\mathrm{Pr}^{0.4}$ for heating $\mathrm{Nu}_D = 0.023\,\mathrm{Re}_D^{4/5}\,\mathrm{Pr}^{0.3}$ for cooling	0.7 < Pr < 120 $2500 < \mathrm{Re}_D < 1.24x10^5$ $L/D > 60$
3	Kakac [24]	$\mathrm{Nu}_D = 0.023\,\mathrm{Re}_D^{4/5}\,\mathrm{Pr}^{0.4}$ for heating $\mathrm{Nu}_D = 0.026\,\mathrm{Re}_D^{4/5}\,\mathrm{Pr}^{0.4}$ for cooling	
4	Petukhov-Kirillov-Popov [25]	$\mathrm{Nu}_D = \frac{(f/8)\mathrm{Re}_D\,\mathrm{Pr}}{1.07+12.7(f/8)^{1/2}\left(\mathrm{Pr}^{2/3}-1\right)}$ friction factor according Moody diagram smoth pipes $f = \left(1.82\log_{10}\mathrm{Re}_D - 1.64\right)^{-2}$	$0.5 < \mathrm{Pr} < 2000$ $10^4 < \mathrm{Re}_D < 5x10^6$
5	Gnielinski [26]	$\mathrm{Nu}_D = \frac{(f/8)(\mathrm{Re}_D-1000)\mathrm{Pr}}{1+12.7(f/8)^{1/2}\left(\mathrm{Pr}^{2/3}-1\right)}$ friction factor according Moody diagram smoth pipes $f = \left(0.79\ln\mathrm{Re}_D - 1.64\right)^{-2}$	$0.5 < \mathrm{Pr} < 2000$ $10^4 < \mathrm{Re}_D < 5x10^6$

Tab. 5 (Continued)

6	Sleicher-Rouse [27]	$\mathrm{Nu}_D = 5 + 0.015\,\mathrm{Re}_D^a\,\mathrm{Pr}^b$ $a = 0.88 - \frac{0.24}{4+\mathrm{Pr}}$ $\quad b = 0.333 + 0.5e^{-0.6\,\mathrm{Pr}}$	$0.1 < \mathrm{Pr} < 10^4$ $10^4 < \mathrm{Re}_D < 10^6$

6.2.4. Collector heat removal factor F_R

It is convenient to define a quantity that relates the actual useful energy gain of a collector to the useful gain if the whole collector surface were at the fluid inlet temperature. This quantity is called the collector heat removal factor F_R. In equation form it is

$$F_R = \frac{\dot{m}c_f}{A_{abs}U}\left[1 - \exp\left(-\frac{A_{abs}UF'}{\dot{m}c_f}\right)\right] \text{ [-]} \tag{34}$$

where

c_f is specific thermal capacity of fluid, J/kg.K;

$\dot{m}$ total mass flow rate of fluid through solar collector, kg/s.

Collector heat removal factor F_R is equivalent to the effectiveness of a conventional heat exchanger, which is defined as ratio of the actual heat transfer to the maximum possible heat transfer. Maximum possible useful heat gain in a solar collector occurs when the whole absorber is at the inlet fluid temperature (no temperature increase along the riser pipes, minimized heat loss).

6.2.5. Incident angle modifier K_{net}

The collector absorbs only a portion of the solar irradiance due to the optical properties of the transparent cover and absorber plate, which are described in the $\tau_n\alpha_{abs}$ and the *IAM* parameters for each irradiance component (K_{beam}, K_{sky}, K_{gnd}). Incident angle modifiers are calculated separately for beam (G_{beam}), sky (G_{sky}) and ground radiation (G_{gnd}). The net incident angle modifier for all incident radiation is calculated by weighting each component by the corresponding modifier.

$$K_{net} = \frac{G_{beam}K_{beam} + G_{sky}K_{sky} + G_{gnd}K_{gnd}}{G_t} \quad \text{[-]} \tag{35}$$

where

G_t total radiation for collector surface, W/m^2.

$$G_t = G_{beam} + G_{sky} + G_{gnd} \quad \text{[W/m}^2\text{]} \tag{36}$$

Incidence angle modifier of solar collector for beam radiation component can be determined by experiment an empirical expression for K_{beam}.

$$K_{beam} = 1 - b_0\left(\frac{1}{\cos\theta} - 1\right) - b_1\left(\frac{1}{\cos\theta} - 1\right)^2 \quad \text{[-]} \tag{37}$$

Sky and ground reflected radiation are considered as diffuse isotropic, that means optical properties for this solar radiation components are not considered as incidence angle dependent like for beam radiation but constant. Incidence angle modifier of solar collector for sky and ground radiation components can be approximated using Brandemuehl and Beckman's equations [28] from the K_{beam} characteristic for given effective incident angle:

$$\theta_{eff,sky} = 59.68 - 0.1388\varphi + 0.001497\varphi^2 \quad [°] \tag{38}$$

$$\theta_{eff,gnd} = 90 - 0.5788\varphi + 0.002693\varphi^2 \quad [°] \tag{39}$$

Finally incident angle modifiers for sky-diffuse and ground-reflected radiation are:

$$K_{sky} = 1 - b_0\left(\frac{1}{\cos\theta_{eff,sky}} - 1\right) - b_1\left(\frac{1}{\cos\theta_{eff,sky}} - 1\right)^2 \quad [-] \tag{40}$$

$$K_{gnd} = 1 - b_0\left(\frac{1}{\cos\theta_{eff,gnd}} - 1\right) - b_1\left(\frac{1}{\cos\theta_{eff,gnd}} - 1\right)^2 \quad [-] \tag{41}$$

In the case of $b_1 = 0$, incident angle modifiers for beam, sky and ground radiation have to be calculated by another equations:

$$K_{beam} = 1 - b_0\left(\frac{1}{\max(0.5, \cos\theta)} - 1\right) - \frac{(1-b_0)(\max(60,\theta) - 60)}{30} \quad [-] \tag{42}$$

$$K_{sky} = 1 - b_0\left(\frac{1}{\max(0.5, \cos\theta_{eff,sky})} - 1\right) - \frac{(1-b_0)(\max(60,\theta_{eff,sky}) - 60)}{30} \quad [-] \tag{43}$$

$$K_{gnd} = 1 - b_0\left(\frac{1}{\max(0.5, \cos\theta_{eff,gnd})} - 1\right) - \frac{(1-b_0)(\max(60,\theta_{eff,gnd}) - 60)}{30} \quad [-] \tag{44}$$

6.2.6. Useful heat output of solar collector Q_u

Useful thermal output from solar collector can be defined in three different ways, based on absorber temperature, mean temperature and input temperature.

$$\dot{Q}_u = A_{abs}\left[\tau_n\alpha_{abs}G_tK_{net} - U(\vartheta_{abs} - \vartheta_{amb})\right] \quad [W] \tag{45}$$

$$\dot{Q}_u = A_{abs}F'\left[\tau_n\alpha_{abs}G_tK_{net} - U(\vartheta_m - \vartheta_{amb})\right] \quad [W] \tag{46}$$

$$\dot{Q}_u = A_{abs}F_R\left[\tau_n\alpha_{abs}G_tK_{net} - U(\vartheta_{in} - \vartheta_{amb})\right] \quad [W] \tag{47}$$

This Type uses Equation (47) for calculation of useful thermal output.

6.2.7. Efficiency of solar collector η

Collector efficiency is defined as usable thermal power output from the collector related to solar radiation input incident on front part of collector (gross area A_G) [29]. Collector efficiency can be related to:

mean absorber temperature $$\eta_{abs} = \frac{A_{abs}}{A_G}\left[\tau_n\alpha_{abs} - \frac{U(\vartheta_{abs} - \vartheta_{amb})}{G_t K_{net}}\right] \quad [-] \quad (48)$$

mean fluid temperature $$\eta_m = F' \frac{A_{abs}}{A_G}\left[\tau_n\alpha_{abs} - \frac{U(\vartheta_m - \vartheta_{amb})}{G_t K_{net}}\right] \quad [-] \quad (49)$$

input fluid temperature $$\eta_{in} = F_R \frac{A_{abs}}{A_G}\left[\tau_n\alpha_{abs} - \frac{U(\vartheta_{in} - \vartheta_{amb})}{G_t K_{net}}\right] \quad [-] \quad (50)$$

This Type uses Equation (57) for calculation of useful thermal output.

6.2.8. Recalculation of fluid ϑ_{mean} and absorber temperature ϑ_{abs}

Since useful heat output, collector heat removal factor and collector efficiency factor have been calculated for first estimates of temperatures, next iteration step should follow.

To calculate heat transfer coefficients at main surfaces of solar collector and to assess the overall collector heat loss coefficient U (external energy balance) in the next iteration step the absorber temperature should be identified from input temperature

$$\vartheta_{abs} = \vartheta_{in} + \frac{\dot{Q}_u}{F_R U A_{abs}}(1 - F_R) \quad [K] \quad (51)$$

Mean fluid temperature ϑ_{mean} necessary for calculation of convection heat transfer coefficient h_i for fluid in pipes in the next iteration step can be obtained from input temperature

$$\vartheta_{mean} = \vartheta_{in} + \frac{\dot{Q}_u}{F_R U A_{abs}}\left(1 - \frac{F_R}{F'}\right) \quad [K] \quad (52)$$

6.3. Iteration loop

Both external and internal energy balances are mutually dependent. Overall collector heat loss coefficient U as main output from external balance is one of the inputs for internal balance. On the other side, mean absorber temperature ϑ_{abs} as one of the outputs from internal balance is used as necessary input for external balance. Iteration loop has been introduced to transfer the results from external balance to starting internal balance and the results from internal balance are put to external balance. Loop iterates as long as the difference between absorber temperatures calculated in two adjacent iteration steps is higher than the required minimum (see Fig. 8).

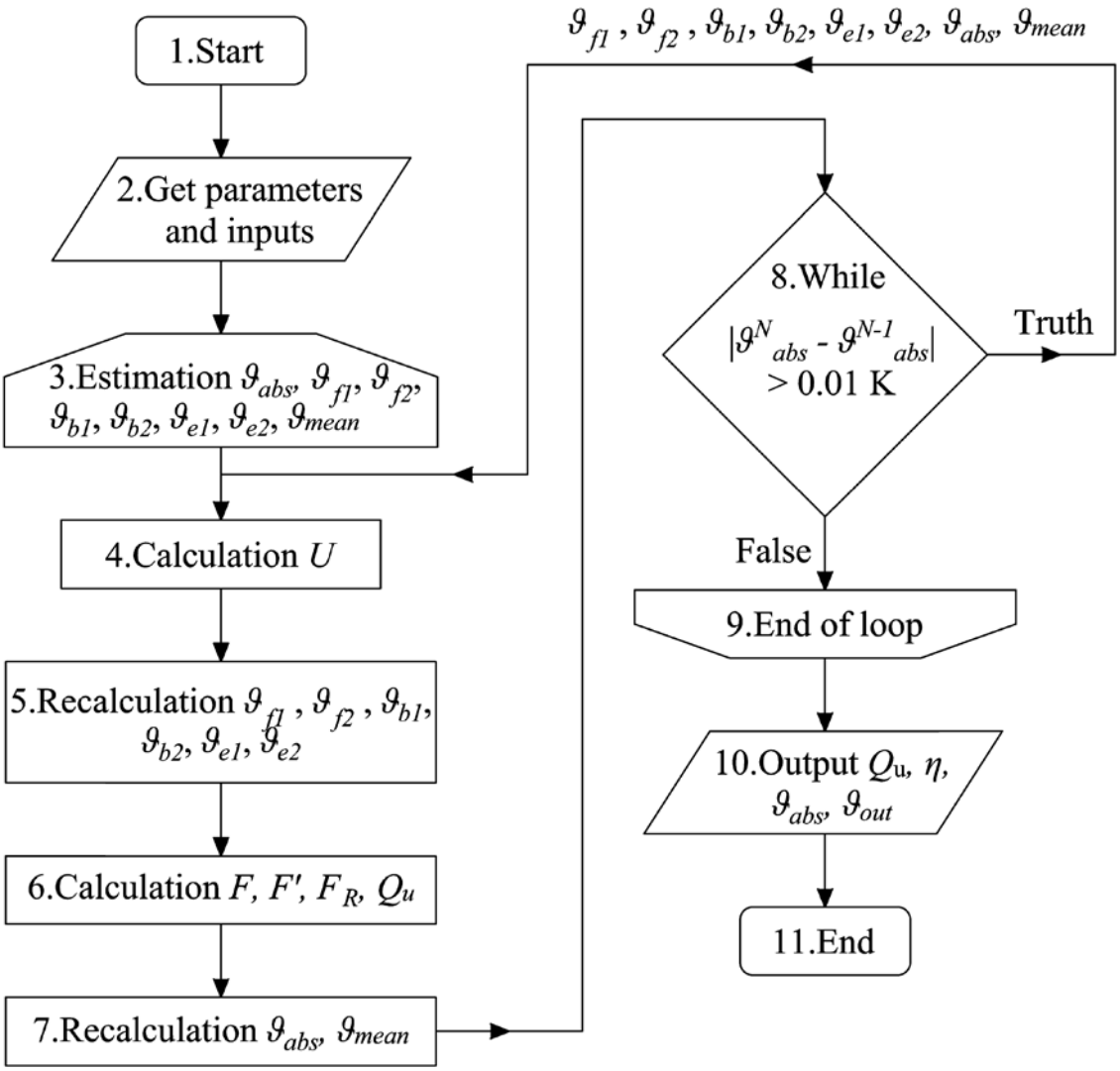

Fig. 8 – Flow chart of the iteration loop

6.4. Experimental validation

The model has been experimentally validated in the frame of solar collectors testing according to the European standard EN ISO 9806 [29] in the accredited Solar Laboratory operated under the University Centre for Energy Efficient Buildings, Czech Technical University in Prague. Solar thermal collectors have been tested to obtain steady-state thermal output at constant operation conditions of inlet temperature (±0.05 K) and mass flow rate (±0.002%) of heat transfer fluid (water) entering collector and at constant climatic conditions of solar irradiation (±1.4%) and ambient temperature (±0.05 K).

Instantaneous efficiency has been calculated from collector thermal output related to total solar irradiation input (incident on collector reference area: gross area). Experimental data points of solar collector efficiency are coupled with uniform uncertainty bars in the graphs. Expanded uncertainty of efficiency and reduced temperature difference have been assessed for experimental data from both type A (statistical) and type B (instrumental) uncertainties considering the coverage factor with 95% level of confidence (normal distribution).

The theoretical calculation of efficiency characteristic by the model is subjected to the uncertainty of real collector parameters which are used as inputs for the model. While geometrical parameters are easily available with high degree of confidence, the number of parameters defining the properties of collector parts is found uncertain within narrow range (e.g., absorber and glazing optical parameters, mostly ±2%), middle range (e.g., conductivity of insulation layer dependent on its temperature and density, ±10%), and quite broad range (e.g., emittance of absorber back side and emittance of insulation layer or collector frame, >10%). Therefore, the results of theoretical calculation could be presented as two delimiting curves where the collector efficiency values can be found in reality.

The mathematical model has been validated in the field of atmospheric solar flat plate collectors (top quality solar collectors with state-of-the-art copper laser-welded absorber coated with a high-performance selective coating and solar glazing as a transparent cover). Four different solar collectors have been used for detailed model validation. The majority of solar thermal collector parameters (e.g., thermal conductivity of insulation, the solar transmittance of the glazing, and the emissivity of the absorber) have been measured experimentally to reduce the uncertainty range. The model has also been tested in the case of various values of slope, mass flow rate, wind velocity, and incident radiation. More information about model validation can be found in Shemelin and Matuska [1]. Fig. 9 shows experimentally measured efficiency points and theoretically modeled efficiency characteristics. It is evident from the results that simulated efficiency characteristics fit the measurements relatively well, which gives confidence about the developed model.

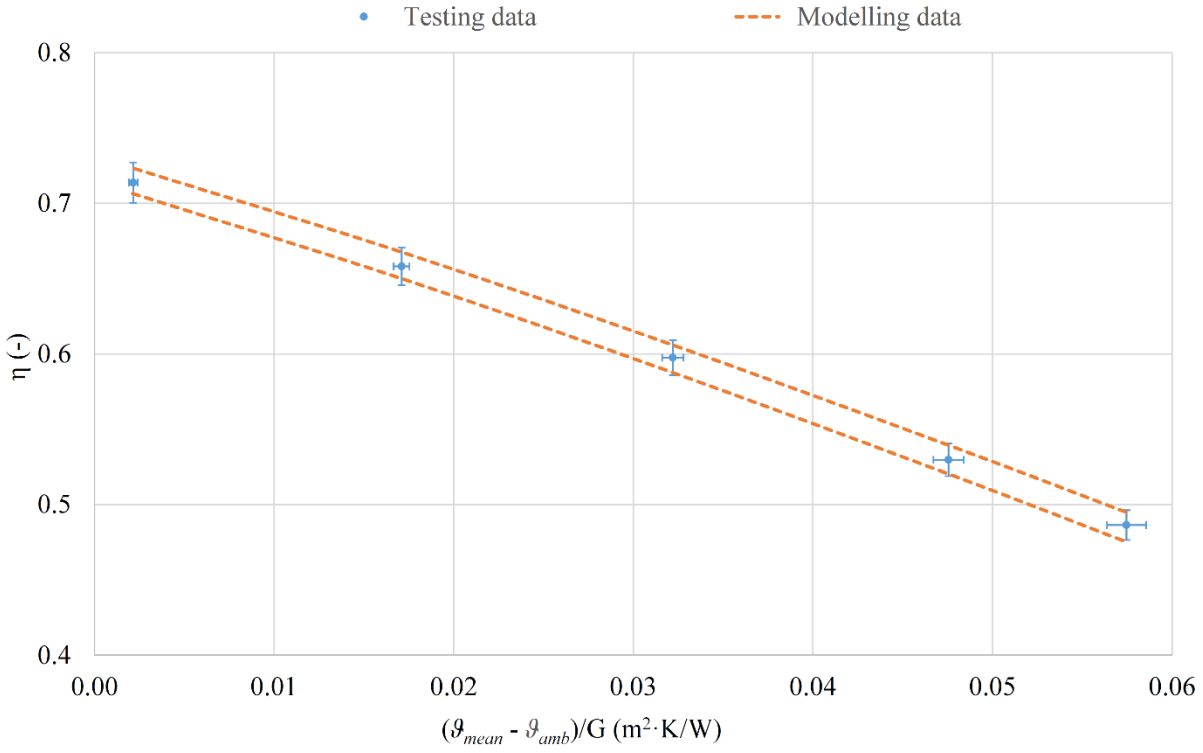

Fig. 9 – Mathematical model validation

7. Operation mode = 1 (Solar air collector)

The core of the Operation mode = 1 is a mathematical model for air solar collector solving one-dimensional heat transfer balances. The thermal networks for two designs of solar collectors considered are shown in Fig. 10.

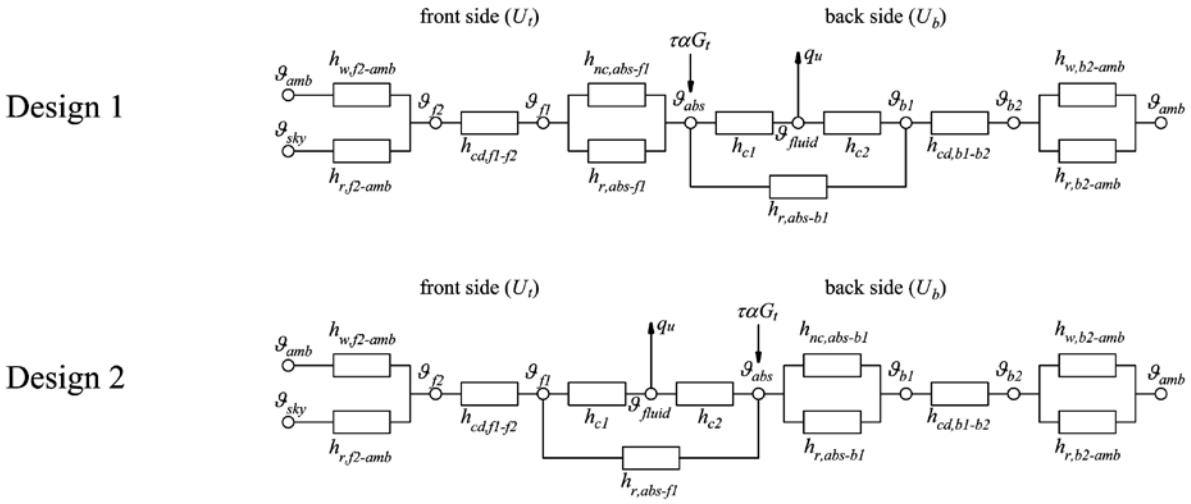

Fig. 10 – Thermal network for solar air collectors

To illustrate the procedure for deriving of usable heat gain Q_u, efficiency with respect to reference collector area (gross area A_G), and output heat transfer fluid temperature t_{out}, we derive equations for the most common design of air collector – Design 1 in **Chyba! Nenalezen zdroj odkazů.**0. The equations for the second design is derived in a similar manner.

Because heat transfer coefficients are temperature dependent, a set of mean temperatures is approximated which allows the heat transfer coefficients to be evaluated as a first guess:

$$\vartheta_{fluid} = \vartheta_{in} + 20 \qquad [\mathrm{K}] \qquad (53)$$

$$\vartheta_{abs} = \vartheta_{in} + 10 \qquad [\mathrm{K}] \qquad (54)$$

Then the surface temperatures are estimated from temperature difference between absorber and ambient environment uniformly as follows:

$$\vartheta_{f1} = \vartheta_{b1} = \vartheta_{abs} - \frac{\vartheta_{abs} - \vartheta_{amb}}{3} \qquad [\mathrm{K}] \qquad (55)$$

$$\vartheta_{f2} = \vartheta_{b2} = \vartheta_{amb} + \frac{\vartheta_{abs} - \vartheta_{amb}}{3} \qquad [\mathrm{K}] \qquad (56)$$

After that heat transfer coefficients can be calculated and collector heat loss coefficients U_t (top) and U_b (back) can be obtained. Since these coefficients have been calculated for incorrect temperatures, next iteration step follows. From heat transfer coefficients and heat flows through front and back side of collector the temperature distribution can be obtained by reverse calculation process. To evaluate the new mean temperatures two different calculation Modes are used (M_8). Mode 1 is based on the Hottel-Whiller-Bliss [3–5,30] general equation for solar collector performance. Mode 2 uses the heat balances equations for each temperature level and matrix inversion method. The newly-calculated mean temperatures are then compared with the

initially-guessed temperatures. The iterative process is repeated until all consecutive results of mean temperatures differ by less than 0.01 K. The scheme of iteration loop is outlined in Fig. 11.

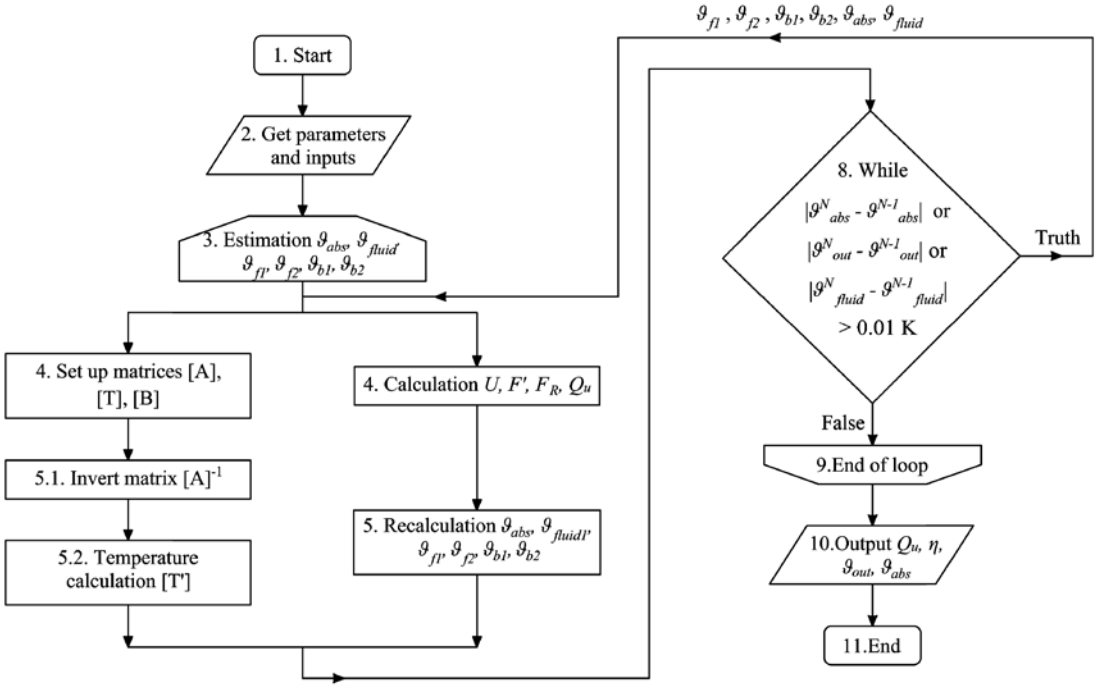

Fig. 11 – Flow chart of iteration loop

7.1. Radiation heat transfer between top surface and sky

Radiation heat transfer between top surface and sky can be determined identically as in 6.1.1.

7.2. Wind convection heat transfer from top, bottom and edge surfaces to ambient

Wind convection heat transfer from top, bottom and edge surfaces to ambient can be determined identically as in 6.1.2.

7.3. Conduction through transparent cover and insulation material

Thermal conductance of the transparent cover and insulation material can be determined identically as in 6.1.3.

7.4. Natural convection in closed gas layer between absorber and transparent cover

Natural convection in closed gas layer between absorber and transparent cover can be determined identically as in 6.1.4.

7.5. Forced convection between parallel plates

To handle forced convection between two parallel plates, both correlations developed especially for parallel plates and many correlations developed for circular tubes may be applied. In both cases, an effective diameter should be used as the characteristic length. It is termed the hydraulic diameter and it is defined as

$$D_h = \frac{4A}{P} \quad [\text{m}] \tag{57}$$

where

A is the flow cross-sectional area, m^2;

P the perimeter wetted by fluid, m.

Then forced convection heat transfer coefficient is determined from Nusselt number

$$h_c = \text{Nu}_D \frac{\lambda_f}{D_h} \ [\text{W/m}^2.\text{K}] \tag{58}$$

where

λ_f is thermal conductivity of heat transfer fluid, W/m.K;

In the presented model the coefficients for both upper and lower surfaces of each channel are assumed equal, $h_{c1} = h_{c2}$ and $h_{c3} = h_{c4}$.

7.5.1. Turbulent flow region (Re > 10000)

Turbulent forced convection heat transfer is widely described. Tab. 6 shows correlations for Nusselt number for turbulent forced convection heat transfer found in the literature.

Tab. 6 – Selected correlations for turbulent flow region

M9	**Author**	**Equation**	**Comment**
1	Kays and Crawford [31]	$\text{Nu}_D = 0.0158\,\text{Re}_D^{0.8}$	developed for solar air collectors, Re > 3000
2	Tan and Charters [32]	$\text{Nu}_D = 0.018\,\text{Re}_D^{0.8}\,\text{Pr}^{0.4}$	developed for solar air collectors, 9500 < Re < 22000
3	Nusselt [33]	$\text{Nu}_D = 0.036\,\text{Re}_D^{0.8}\,\text{Pr}^{1/3}\left(D_h/L\right)^{0.055}$	developed for circular tube, 10 < L/D < 400
4	Sieder and Tate [20]	$\text{Nu}_D = 0.027\,\text{Re}_D^{0.8}\,\text{Pr}^{1/3}\left(\mu/\mu_w\right)^{0.14}$	developed for circular tube, Re > 10000
5	Dittus-Boelter [23]	$\text{Nu}_D = 0.0243\,\text{Re}_D^{4/5}\,\text{Pr}^{0.4}$ for heating $\text{Nu}_D = 0.0265\,\text{Re}_D^{4/5}\,\text{Pr}^{0.3}$ for cooling	developed for circular tube, Re > 10000
6	Gnielinski [26]	$\text{Nu}_D = \frac{(f/8)(\text{Re}_D - 1000)\,\text{Pr}}{1 + 12.7(f/8)^{1/2}\left(\text{Pr}^{2/3} - 1\right)}$ friction factor according to Moody´s diagram smoth pipes $f = \left(1.82\log_{10}\text{Re}_D - 1.64\right)^{-2}$	developed for circular tube, more accurate, 3000 < Re < 5 x 106

Tab. 6 (Continued)

7	Petukhov [25]	$\mathrm{Nu}_D = \dfrac{(f/8)\,\mathrm{Re}_D\,\mathrm{Pr}}{1+12.7(f/8)^{1/2}(\mathrm{Pr}^{2/3}-1)}$ friction factor according to Moody´s diagram smoth pipes $f = (1.82\log_{10}\mathrm{Re}_D - 1.64)^{-2}$	circular tube, more accurate, 3000 < Re < 5 x 10^6

7.5.2. Transition flow region (2300 < Re < 6000)

Hausen [19] presented the following empirical correlation for the average Nusselt number beginning of the heated section and the position L for flow in a tube:

$$\mathrm{Nu}_D = 0.116\left(\mathrm{Re}_D^{2/3} - 125\right)\mathrm{Pr}^{1/3}\left[1 + (D_h/L)^{2/3}\right](\mu/\mu_w)^{0.14} \qquad [-] \qquad (59)$$

7.5.3. Laminar flow region (Re < 2300)

For laminar flow, the use of circular tube correlations is less accurate, particularly for cross sections characterized by sharp corners. For such cases the Nusselt number corresponding to fully developed conditions may be obtained from the following empirical correlation developed for laminar flow between two parallel flat plates with one side insulated and the other subjected to a constant heat flux [34]:

$$\mathrm{Nu}_D = 5.4 + \frac{0.0019\left[\mathrm{Re}\,\mathrm{Pr}(D_h/L)\right]^{1.71}}{1 + 0.00563\left[\mathrm{Re}\,\mathrm{Pr}(D_h/L)\right]^{1.17}} \qquad [-] \qquad (60)$$

7.6. Natural convection between absorber and back insulation

Natural convection in closed gas layer between absorber and back insulation cover can be determined identically as in 6.1.6.

7.7. Radiation heat exchange between frame and adjacent ambient surfaces

Radiation heat transfer coefficient between exterior surface of collector back frame and adjacent surfaces in ambient environment (roof) related to ambient temperature ϑ_{amb} can be expressed as

$$h_{r,b2-amb} = \frac{\sigma}{\dfrac{1}{\varepsilon_{b2}} + \dfrac{1}{\varepsilon_{as}} - 1}\,\frac{\vartheta_{b2}^4 - \vartheta_{amb}^4}{\vartheta_{b2} - \vartheta_{amb}} \qquad [\mathrm{W/m^2.K}] \qquad (61)$$

7.8. Reverse temperature calculation

7.8.1. Mode 1

In steady state, the performance of a solar collector is described by an energy balance that indicates the distribution of incident solar energy into useful energy gain, thermal losses, and optical losses. The solar radiation absorbed by a collector per unit area of absorber A_{abs} is equal to the difference between the incident solar radiation and the optical. The thermal energy lost from the collector to the surroundings by conduction, convection, and infrared radiation can be represented as the product of heat transfer coefficient U, times the difference between the mean fluid temperature ϑ_{fluid} and the ambient temperature ϑ_{amb}:

$$\dot{Q}_u = A_{abs} F' \left[\tau_n \alpha_{abs} G_t - U \left(\vartheta_{fluid} - \vartheta_{amb} \right) \right] \quad [\mathrm{W}] \tag{62}$$

The problem with this equation is that the overall heat loss coefficient U and the collector efficiency factor F' is difficult to calculate. The algebra is somewhat tedious and only results of deriving F' and U are presented in Fig. 12. More information about F' and U deriving can be found in Duffie and Beckman [6].

Design 1

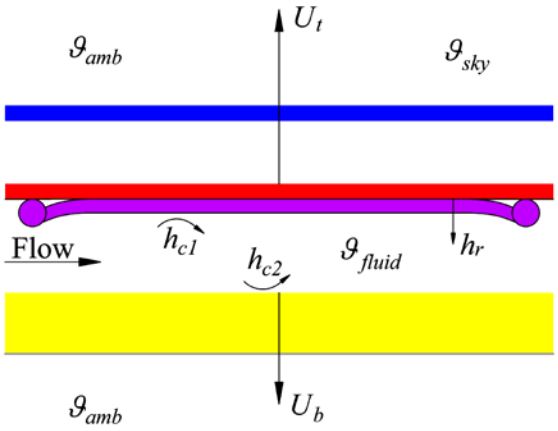

$$U = U_t + U_b \quad [\mathrm{W/m^2.K}] \tag{63}$$

$$F' = \frac{1}{1 + \dfrac{U}{h_{c1} + \dfrac{1}{\dfrac{1}{h_{c2}} + \dfrac{1}{h_{r,abs-b1}}}}} \quad [-] \tag{64}$$

Design 2

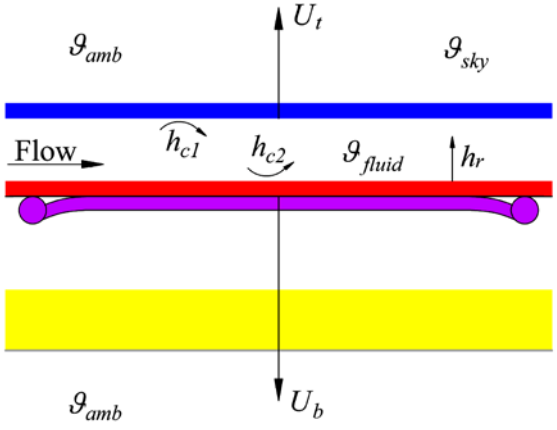

$$U = \frac{\left(U_b + U_t\right)\left(h_{c1}h_{c2} + h_{r,abs-f1}h_{c1} + h_{r,abs-f1}h_{c2}\right) + U_b U_t \left(h_{c1} + h_{c2}\right)}{h_{c1}h_{r,abs-f1} + h_{c2}U_t + h_{c2}h_{r,abs-f1} + h_{c1}h_{c2}} \quad [\mathrm{W/m^2.K}] \tag{65}$$

$$F' = \frac{h_{r,abs-f1}h_{c1} + h_{c2}U_t + h_{c2}h_{r,abs-f1} + h_{c1}h_{c2}}{\left(U_t + h_{r,abs-f1} + h_{c1}\right)\left(U_b + h_{c2} + h_{r,abs-f1}\right) - h_{r,abs-f1}^2} \quad [-] \tag{66}$$

Fig. 12 – Overall heat loss coefficients and efficiency factors for different solar air collector designs

After that the collector flow factor F'' and the collector heat removal factor F_R can be obtained as follows

$$F'' = \frac{\dot{m}c_f}{A_{abs}UF'}\left[1-\exp\left(-\frac{A_{abs}U}{\dot{m}c_f F'}\right)\right] \quad [-] \quad (67)$$

where

c_f is specific thermal capacity of fluid, J/kg.K;

$\dot{m}$ total mass flow rate of fluid through air channel, kg/s,

$$F_R = F''F' \quad [-] \quad (68)$$

Then the useful energy gain is determined

$$\dot{Q}_u = A_{abs}F_R\left[\tau_n\alpha_{abs}G_t - U\left(\vartheta_{in}-\vartheta_{amb}\right)\right] \quad [W] \quad (69)$$

and the outlet temperature

$$\vartheta_{out} = \vartheta_{in} + \frac{\dot{Q}_u}{\dot{m}c_f} \quad [K] \quad (70)$$

Since the useful heat energy gain, the collector heat removal factor and the collector efficiency factor have been calculated for first estimates of temperatures, next iteration step should follow. To calculate heat transfer coefficients at main surfaces of solar collector and to assess the overall collector heat loss coefficient U in the next iteration step the absorber temperature, the mean fluid temperature, and the temperature distribution should be derived

$$\vartheta_{abs} = \vartheta_{in} + \frac{\dot{Q}_u}{F_R UA_{abs}}\left(1-F_R\right) \quad [K] \quad (71)$$

$$\vartheta_{fluid} = \vartheta_{in} + \frac{\dot{Q}_u}{F_R UA_{abs}}\left(1-F'''\right) \quad [K] \quad (72)$$

$$\vartheta_{f1} = \frac{\vartheta_{abs}\left(h_{r,abs-f1}+h_{nc}\right)-U_t\left(\vartheta_{abs}-\vartheta_{amb}\right)}{h_{r,abs-f1}+h_{nc}} \quad [K] \quad (73)$$

$$\vartheta_{f2} = \frac{\vartheta_{f2}h_{cd,f1-f2}-U_t\left(\vartheta_{abs}-\vartheta_{amb}\right)}{h_{cd,f1-f2}} \quad [K] \quad (74)$$

$$\vartheta_{b1} = \frac{\vartheta_{fluid}h_{c2}+\vartheta_{abs}h_{r,abs-b2}+U_b\vartheta_{amb}}{h_{c2}+h_{r,abs-b1}+U_b} \quad [K] \quad (75)$$

$$\vartheta_{b2} = \frac{\vartheta_{b1}h_{cd,b1-b2}-U_b\left(\vartheta_{b1}-\vartheta_{amb}\right)}{h_{cd,b1-b2}} \quad [K] \quad (76)$$

7.8.2. Mode 2

Mode 2 operates in a principally different manner. The core of the Mode 2 is a set of heat balance equations obtained from the thermal network at the points:

$$\vartheta_{f1}: \quad h_{r,f2-amb}\left(\vartheta_{f2}-\vartheta_{sky}\right)+h_{w,f2-amb}\left(\vartheta_{f2}-\vartheta_{amb}\right)=h_{cd,f1-f2}\left(\vartheta_{f1}-\vartheta_{f2}\right) \tag{77}$$

$$\vartheta_{f2}: \quad h_{cd,f1-f2}\left(\vartheta_{f1}-\vartheta_{f2}\right)=h_{r,abs-f1}\left(\vartheta_{abs}-\vartheta_{f1}\right)+h_{nc}\left(\vartheta_{abs}-\vartheta_{f1}\right) \tag{78}$$

$$\vartheta_{abs}: \quad \tau\alpha GK_{net}=\left(h_{r,abs-f1}+h_{nc}\right)\left(\vartheta_{abs}-\vartheta_{f1}\right)+h_{r,abs-b1}\left(\vartheta_{abs}-\vartheta_{b1}\right)+h_{c1}\left(\vartheta_{abs}-\vartheta_{fluid}\right) \tag{79}$$

$$\vartheta_{fluid}: \quad h_{c1}\left(\vartheta_{abs}-\vartheta_{fluid}\right)=h_{c2}\left(\vartheta_{fluid}-\vartheta_{b2}\right)+\frac{2mc_f}{ac}\left(\vartheta_{fluid}-\vartheta_{in}\right) \tag{80}$$

$$\vartheta_{b2}: \quad h_{r,abs-b1}\left(\vartheta_{abs}-\vartheta_{b1}\right)+h_{c2}\left(\vartheta_{fluid}-\vartheta_{b1}\right)=h_{cd,b1-b2}\left(\vartheta_{b1}-\vartheta_{b2}\right) \tag{81}$$

$$\vartheta_{b1}: \quad h_{cd,b1-b2}\left(\vartheta_{b1}-\vartheta_{b2}\right)=h_{r,b2-amb}\left(\vartheta_{b2}-\vartheta_{amb}\right)+h_{w,b2-amb}\left(\vartheta_{b2}-\vartheta_{amb}\right) \tag{82}$$

By rearranging, we obtain a system of linear equations in the matrix form:

$$\begin{bmatrix} h_{r,f2-amb}+h_{w,f2-amb}+h_{cd,f1-f2} & -h_{cd,f1-f2} & 0 & 0 \\ -h_{cd,f1-f2} & h_{cd,f1-f2}+h_{r,abs-f1}+h_{nc} & -h_{r,abs-f1}-h_{nc} & 0 \\ 0 & -h_{r,abs-f1}-h_{nc} & h_{r,abs-f1}+h_{nc}+h_{r,abs-b1}+h_{c1} & -h_{c1} \\ 0 & 0 & h_{c1} & -h_{c1}-h_{c2}-\frac{2mc_f}{ac} \\ 0 & 0 & h_{r,abs-b1} & h_{c2} \\ 0 & 0 & 0 & 0 \end{bmatrix}$$

$$\begin{bmatrix} 0 & 0 \\ 0 & 0 \\ -h_{r,abs-b1} & 0 \\ h_{c2} & 0 \\ -h_{r,abs-b1}-h_{c2}-h_{cd,b1-b2} & h_{cd,b1-b2} \\ h_{cd,b1-b2} & h_{r,b2-amb}+h_{w,b2-amb}+h_{cd,b1-b2} \end{bmatrix} \begin{bmatrix} \vartheta_{f2} \\ \vartheta_{f1} \\ \vartheta_{abs} \\ \vartheta_{fluid} \\ \vartheta_{b1} \\ \vartheta_{b2} \end{bmatrix} = \begin{bmatrix} h_{r,f2-amb}\vartheta_{sky}+h_{w,f2-amb}\vartheta_{amb} \\ 0 \\ \tau\alpha GK_{net} \\ \frac{2mc_f}{ac}\vartheta_{in} \\ 0 \\ h_{r,b2-amb}\vartheta_{amb}+h_{w,b2-amb}\vartheta_{amb} \end{bmatrix} \tag{83}$$

In general, the above matrices may be displayed as

$$[A][T]=[B] \tag{84}$$

The mean temperature vector may be determined by matrix inversion as

$$[T]=[A]^{-1}[B] \tag{85}$$

Then the outlet fluid temperature and the useful energy gain can be determined

$$\vartheta_{out}=2\vartheta_{fluid}-\vartheta_{in} \qquad [\mathrm{K}] \tag{86}$$

$$\dot{Q}_u=mc_f\left(\vartheta_{fluid}-\vartheta_{in}\right) \qquad [\mathrm{W}] \tag{87}$$

7.9. Iterative procedure

The newly-calculated temperatures values ϑ_{out}, ϑ_{abs}, and ϑ_{fluid} are then compared with previously assumed ones. The iterative process is repeated until all consecutive outlet temperatures, absorber temperatures, and heat transfer fluid temperatures differ by less than 0.01 K. Normally, the number of iterations required is not more than four or five.

7.10. Instantaneous efficiency

Finally, the instantaneous solar air collector efficiency is

$$\eta = \frac{\dot{Q}_u}{A_G G_t} \qquad [-] \qquad (88)$$

where

G_t is total radiation for collector surface, W/m^2;

$$G_t = \left(G_{beam} + G_{sky} + G_{gnd}\right) K_{net} \qquad [\mathrm{W/m^2}] \qquad (89)$$

where

K_{net} is net incident angle modifier.

7.11. Incident angle modifier K_{net}

Incident angle modifier can be determined identically as in 6.2.5.

7.12. Experimental validation (to be added in 2018)

8. References

[1] Shemelin V, Matuska T. TRNSYS type 205-Model of glazed solar liquid collector based on detailed construction parameters and energy balance 2017:34.

[2] Shemelin V, Matuska T. TRNSYS type 206-Model of glazed solar air collector based on detailed construction parameters and energy balance 2017:19.

[3] Hottel H, Woertz B. Performance of flat-plate solar-heat collectors. Trans ASME (Am Soc Mech Eng); (United States) 1942;64:91–104.

[4] Hottel H, Whillier A. Evaluation of flat-plate solar collector performance. Trans Conf Use Sol Energy; 1955;3:74–104.

[5] Bliss Jr. RW. The derivations of several “Plate-efficiency factors” useful in the design of flat-plate solar heat collectors. Sol Energy 1959;3:55–64. doi:10.1016/0038-092X(59)90006-4.

[6] Duffie JA, Beckman WA. Solar engineering of thermal processes. John Wiley & Sons; 2013.

[7] Mcadams WH. Heat Transmission 3d Ed. New York: McGraw-Hill; 1954.

[8] J. H. DW, W. W. S. C, Proctor. Solar and wind induced external coefficients for solar collectors. Coop Mediterr Pour l’Energie Solaire, Rev Int d’Heliotechnique 1977;2:56.

[9] Test FL, Lessmann RC. An Experimental Study of Heat Transfer During Forced Convection over a Rectangular Body. J Heat Transfer 1980;102:146–51.

[10] Test FL, Lessmann RC, Johary A. Heat Transfer During Wind Flow over Rectangular Bodies in the Natural Environment. J Heat Transfer 1981;103:262–7.

[11] Kumar S, Sharma VB, Kandpal TC, Mullick SC. Wind induced heat losses from outer cover of solar collectors. Renew Energy 1997;10:613–6. doi:10.1016/S0960-1481(96)00031-6.

[12] Hollands KGT, Unny TE, Raithby GD, Konicek L. Free Convective Heat Transfer Across Inclined Air Layers. J Heat Transfer 1976;98:189–93.

[13] Buchberg H, Catton I, Edwards DK. Natural Convection in Enclosed Spaces - A Review of Application to Solar Energy Collection. J Heat Transfer 1976;98:182–8.

[14] Randall KR, Mitchell JW, El-Wakil MM. Natural Convection Heat Transfer Characteristics of Flat Plate Enclosures. J Heat Transfer 1979;101:120–5.

[15] Schinkel W. Natural concection in inclined air-filled enclosures. Delft: Dutch Efficiency Bureau - Pijnacker; 1980.

[16] Niemann H. Die Wärmeübertragung durch natürliche Konvektion in spaltförmigen Hohlräumen. Gesund Ing 1948;69:224–8.

[17] Matuska T, Zmrhal V. A mathematical model and design tool KOLEKTOR 2.2 reference handbook. Prague: 2009.

[18] Shah RK, London AL. Lanimar flow forced convection in duts: a source book for compact heat exchanger analytical data. Academic press; 1978.

[19] Hausen H. Darstellung des Warmeuberganges in Rohren durch verallgemeinerte Potenzbeziehungen. Z VDI Beih Verfahrenstech 1943;4:91–8.

[20] Sieder EN, Tate GE. Heat Transfer and Pressure Drop of Liquids in Tubes. Ind Eng Chem 1936;28:1429–35. doi:10.1021/ie50324a027.

[21] Churchill SW, Chu HHS. Correlating equations for laminar and turbulent free convection from a vertical plate. Int J Heat Mass Transf 1975;18:1323–9.

[22] Colburn AP. A method of correlating forced convection heat-transfer data and a comparison with fluid friction. Int J Heat Mass Transf 1964;7:1359–84.

[23] Dittus FW, Boelter LMK. Heat transfer in automobile radiators of the tubular type. Int Commun Heat Mass Transf 1985;12:3–22.

[24] Kakaç S, Shah RK, Aung W, others. Handbook of single-phase convective heat transfer. Wiley New York et al.; 1987.

[25] Petukhov BS. Heat transfer and friction in turbulent pipe flow with variable physical properties. Adv Heat Transf 1970;6:503–64.

[26] Gnielinski V. New equations for heat and mass transfer in turbulent pipe and channel flow. Int Chem Eng 1976;16:359–68.

[27] Sleicher C, Rouse MW. A convenient correlation for heat transfer to constant and variable property fluids in turbulent pipe flow. Int J Heat Mass Transf 1975;18:677–83.

[28] Brandemuehl MJ, Beckman WA. Transmission of diffuse radiation through CPC and

flat plate collector glazings. Sol Energy 1980;24:511–3.

[29] ISO. 9806: 2013. Sol Energy--Solar Therm Collect Methods 2013.

[30] Smith CC, Weiss TA. Design application of the Hottel-Whillier-Bliss equation. Sol Energy 1977;19:109–13. doi:10.1016/0038-092X(77)90047-0.

[31] Kays WM, Crawford ME. Convective Heat and Mass Transfer, 2nd edn McGraw-Hill. New York 1980:141.

[32] Tan HM, Charters WWS. Effect of thermal entrance region on turbulent forced-convective heat transfer for an asymmetrically heated rectangular duct with uniform heat flux. Sol Energy 1969;12:513–6. doi:10.1016/0038-092X(69)90072-3.

[33] Nusselt W. Der Wärmeaustausch zwischen Wand und Wasser im Rohr. Forsch Auf Dem Gebiete Des Ingenieurwesens 1931;2:309–13. doi:10.1007/BF02583210.

[34] Heaton HS, Reynolds WC, Kays WM. Heat transfer in annular passages. Simultaneous development of velocity and temperature fields in laminar flow. Int J Heat Mass Transf 1964;7:763–81. doi:10.1016/0017-9310(64)90006-7.

Appendix 1: Installation

The Type207 dual function solar collector model is a TRNSYS 17 drop-in dll component. For a complete set of files one should have:

Type207.dll – the drop-in dll file

Type207.tmf – the Simulation Studio proforma

Type207.bmp – the Simulation Studio proforma icon

For installation:

1. Copy the .dll file to \TRNSYS17\UserLib\ReleaseDLLs\

2. Copy the .tmf and .bmp files to the \Proformas folder, e.g. C:\Trnsys17\Studio\Proformas\Nonstandard\

3. Restart simulation studio if it was running.